Published in final edited form as:
J Control Release. 2012 August 10; 161(3): 959–966. doi:10.1016/j.jconrel.2012.05.014.

Receptor-mediated transcytosis: a mechanism for active extravascular transport of nanoparticles in solid tumors

Wei Lu[1,#], **Chiyi Xiong**[1], **Rui Zhang**[1], **Lifang Shi**[2], **Miao Huang**[1], **Guodong Zhang**[1], **Shaoli Song**[1], **Qian Huang**[1], **Gang-yu Liu**[2], and **Chun Li**[1,*]

[1]Department of Experimental Diagnostic Imaging, The University of Texas MD Anderson Cancer Center, Houston, Texas 77030, USA

[2]Department of Chemistry, University of California, Davis, California 95616, USA

Abstract

Targeted nanoparticle-based delivery systems have been used extensively to develop effective cancer theranostics. However, how targeting ligands affect extravascular transport of nanoparticles in solid tumors remains unclear. Here, we show, using B16/F10 melanoma cells expressing melanocortin type-1 receptor (MC1R), that the nature of targeting ligands, i.e., whether they are agonists or antagonists, directs tumor uptake and intratumoral distribution after extravasation of nanoparticles from tumor vessels into the extravascular fluid space. Pegylated hollow gold nanospheres (HAuNS, diameter≈40 nm) coated with MC1R agonist are internalized upon ligand-receptor binding, whereas MC1R antagonist-conjugated HAuNS remain attached on the cell surface. Transcellular transport of agonist-conjugated HAuNS was confirmed by a multilayer tumor cell model and by transmission electron microscopy. MC1R agonist- but not MC1R antagonist-conjugated nanoparticles exhibit significantly higher tumor uptake than nontargeted HAuNS and are quickly dispersed from tumor vessels via receptor-mediated endocytosis and subsequent transcytosis. These results confirm an active transport mechanism that can be used to overcome one of the major biological barriers for efficient nanoparticle delivery to solid tumors.

Keywords

Nanoparticles; Melanocortin type-1 receptor (MC1R); Transcytosis; Agonists; Antagonists

1. Introduction

Many targeted nanoparticle-based delivery systems have been developed with the goals of enhancing tumor-specific uptake of nanoparticles, reducing systemic toxicity, and increasing the efficacy of anticancer therapies. However, targeting of nanoparticles to tumor cells, although extremely appealing in this era of personalized medicine, is challenging because of the presence of a number of biological barriers [1]. Furthermore, there has been a lack of comprehensive study of the various factors that contribute to the tumor uptake efficiency of

*Corresponding author: Department of Experimental Diagnostic Imaging, Unit 59, The University of Texas MD Anderson Cancer Center, 1515 Holcombe Boulevard, Houston, Texas 77030. Phone: (713) 792-5182. Fax: (713) 794-5456. cli@mdanderson.org.
#Present address: Department of Biomedical and Pharmaceutical Sciences, College of Pharmacy, The University of Rhode Island, Kingston, Rhode Island 02881, USA.

"active targeting" strategies, in which tumor-specific ligands are used to direct nanoparticles to tumor cells [2]. Pirollo and Chang [2] argue that in some ligand-conjugated nanoparticle systems, tumor uptake may be due at least in part to the enhanced permeability and retention (EPR) effect of long-circulating nanoparticles, which raises the question of whether true targeted delivery has been achieved with many of the purported active targeting nanoparticles. Using 3 different targeting schemes, Huang et al [3] showed that targeting ligands only marginally improve the total accumulation of gold nanorods in xenograft tumor models in comparison with nontargeted controls. Similar observations have been made with other nanoparticle polymers, liposomes, and gold nanoparticles [4–6]. In a study of epithelial growth factor receptor-targeting hollow gold nanospheres (HAuNS), most nanoparticles were distributed to the perivascular region [6]. These data suggest that efficient tumor delivery of targeted nanoparticles is limited by dispersion of nanoparticles in tumor interstitium.

Here, we report that an active transport mechanism, i.e., receptor-mediated transcytosis, can facilitate extravascular transport of nanoparticles and thus can effectively enhance delivery of nanoparticles within the tumor volume. Agonist and antagonist ligands of membrane receptors behave differently upon binding to their targets. An agonist fully activates the receptor upon ligand-receptor interaction and receptor internalization, while an antagonist does not provoke a biological response itself upon binding to a receptor but blocks or dampens agonist-mediated responses. We hypothesized that the nature of targeting ligands attached to the surface of nanoparticles, i.e., whether the ligands are agonists or antagonists, affects extravascular transport and thus the tumor-targeting efficiency of the nanoparticles. To test this hypothesis, we selected melanocortin type-1 receptor (MC1R), one of the 5 subtypes of melanocortin receptors, as a target. MC1R is overexpressed in melanoma cells [7, 8]. Molecular mechanism studies on all subtypes of melanocortin receptors have shown that receptor desensitization, internalization, and downregulation are different with agonists than with antagonists [9, 10] —specifically, melanocortin receptor agonists lead to receptor internalization upon binding, but melanocortin receptor antagonists do not [9, 10]. Therefore, nanoparticle-based delivery systems with MC1R agonists and those with MC1R antagonists may have different effects on the transport of nanoparticles in the extravascular space.

2. Materials and methods

2.1. Conjugation of MC1R agonists and antagonists to HAuNS

HAuNS were synthesized according to our previous report [6, 11]. The MC1R agonist (Ago) and antagonist (Ant) peptides were synthesized manually using Rink amide resin and N^{α}-fluorenylmethyloxycarbonyl chemistry (See Supplementary Information). Both MC1R agonists and antagonists as targeting moieties were linked to HAuNS through poly(ethylene glycol) (PEG) linker (Fig. 1A, Supporting Information). For fluorescence imaging, the HAuNS were labeled with tetramethylrhodamine-PEG_{5000}-thioctic acid (TA-PEG-TMR, Fig. S1). For quantitative analysis and micro-positron emission tomography (microPET) imaging, the above-described HAuNS were labeled with the positron emitter ^{64}Cu ($t_{1/2}$=12.7 h) according to previously reported procedure [12].

2.2. Receptor binding assay

Competitive binding experiments were carried out using murine B16/F10 melanoma cells (ATCC) as previously reported [13]. B16/F10 cells were seeded on 24-well plates 48 h before assay (20,000 cells/well). The cell culture medium was aspirated, and cells were washed twice with a freshly prepared binding buffer containing DMEM/F12 medium, 25 mM HEPES (pH 7.4), and 0.2% bovine serum albumin (BSA). For peptide competition,

cells were incubated with different concentrations of unlabeled Ago or Ant and labeled [^{125}I]-NDP-α-MSH (0.1 μCi/well, Perkin-Elmer Life Science, Waltham, MA) for 40 min at 4°C. For particle competition, different concentrations of unlabeled HAuNS conjugates were used with [^{125}I]-NDP-α-MSH. For nonspecific binding, an excessive amount of Ago, i.e., 200 μg/ml NDP-α-MSH, was used. After incubation, the assay medium was removed, and each well was washed 3 times with the binding buffer. The cells were then lysed by the addition of 250 μL of CelLytic M cell lysis reagent (Sigma). The radioactivity of the lysis solution was measured using a Packard Cobra gamma counter. IC_{50} estimates and their associated standard errors were determined by fitting the data using a nonlinear least squares analysis using GraphPad Prism 5 software (GraphPad).

2.3. Immunofluorescence microscopy

For visualization of intracellular translocation of MC1R, transient transfection of plasmid construct encoding GFP-tagged open reading frame clone of *Homo sapiens* MC1R (Origene) was carried out using Lipofectamine 2000 reagent (Invitrogen) as recommended by the manufacturer. Briefly, human embryonic kidney (HEK) 293 cells (ATCC) were seeded on 100-mm plates 1 day before transfection. The plasmid DNA encoding gene comprised of *green fluorescent protein* (*GFP*) and *MC1R* (5 μg) was mixed with Lipofectamine 2000 reagent in serum-free medium, incubated at room temperature for 30 minutes, and then added to the cells. Four hours after the addition of the plasmid DNA, the transfection mixture was replaced with DMEM/F12 medium supplemented with 10% fetal bovine serum (FBS). The cells were then incubated for an additional 24 hours. The transfection efficiency was examined under a fluorescence microscope and was found to be greater than 95%.

The MC1R-GFP-transfected HEK 293 cells were trypsinized and seeded (1×10^4) in an 8-well Lab-Tek II chambered coverglass (Thermo Fisher Scientific) 48 h before the experiment. The cells were incubated with different tetramethylrhodamine-labeled HAuNS conjugates (2×10^9 nanoparticles/ml) for 20 min at 37°C with or without the presence of 200 μg/ml free Ant (blocking). After washing in PBS, the cells were directly visualized under an Olympus Fluoview FV1000 confocal laser scanning microscope (FV1-ASW, Olympus) equipped with a fluorescein isothiocyanate filter for MC1R-GFP and a rhodamine filter for nanoparticles.

2.4. Atomic force microscopy (AFM) imaging

For AFM imaging, B16/F10 cells were seeded on a petri dish (MatTek Corporation) 24 h before assay. The cell culture medium was aspirated, and cells were washed twice with DMEM/F12 medium. Cells were incubated in medium (untreated cells), medium containing 1.5×10^{11}/ml HAuNS conjugates for 1 h inside a standard incubator (NAPCO 800 WJ, Thermo Electron Corporation) at 37°C in an environment of 5% CO_2. After treatment, cells were fixed using a 3.7% formaldehyde solution (Fisher Scientific) for 30 min and then rinsed and stored in PBS until AFM study. AFM imaging was performed using a deflection type instrument (MFP3D, Asylum Research Inc.). All images were acquired in PBS solution. For morphology studies or large area scans, contact mode was employed to characterize the cellular surfaces. The probe was a silicon cantilever (CSC38 lever B, MikroMasch) with a force constant of $k = 0.03$ N/m. The imaging force was controlled to be <1 nN as determined from the force-distance curve [14, 15]. For high-resolution imaging, tapping mode was employed using silicon nitride cantilevers (Biolever B, Olympus) with a force constant of $k = 0.03$ N/m. The driving frequency was typically 6–8 kHz. The imaging set point was adjusted to 60% damping of the amplitude.

2.5. Transcytosis of HAuNS in vitro

An *in vitro* multilayer tumor cell model was established via seeding of B16/F10 cells (6,000/well) in 24-well Falcon cell culture inserts with 1-μm-diameter microporous poly-(ethylene terephthalate) membrane (Becton Dickinson). After 72 h, the cells formed 2–3 layers. DMEM/F12 medium plus 0.2% BSA was added to the lower compartments of 24-well plates (0.7 ml per well), i.e., the basolateral side. The medium containing ^{64}Cu-labeled HAuNS conjugates (2×10^9 nanoparticles/ml; 2 μCi, 0.2 ml) was added in the upper compartment, i.e., the apical side, at time 0. The study was performed on a rocking platform at 37°C. At 15, 30, 45, and 60 min after addition of nanoparticles, the cell culture insert was transferred to another well of a 24-well plate containing 0.7 ml of medium. For the inhibition experiment, free Ant with 200 μg/ml final concentration was additionally added to the nanoparticle solution. The medium from each lower compartment and 2 μl from the initial solution containing ^{64}Cu-labeled HAuNS in the upper compartment were transferred and measured using the gamma counter. The inserts without cell growth were used as control. Triplicate samples were measured. Permeability coefficients (P) of the nanoparticles were calculated according to the following equation [16, 17]

$$P=\frac{\Delta Q/\Delta t}{C_0\times A} \quad \text{(eq. 1)}$$

where $\Delta Q/\Delta t$ indicates the linear appearance rate of mass in the lower compartment; C_0 indicates the initial nanoparticle concentration in the upper compartment; and A represents the membrane surface area of the cell culture insert, i.e., 0.3 cm^2. The permeability calculated from the cell culture insert with multiple layers of cells was denoted P_t, whereas the permeability calculated from the cell culture insert without cell growth (the control filter) was denoted P_f. The permeability for the cell multilayer alone (P_c) was calculated from [18, 19]

$$\frac{1}{P_c}=\frac{1}{P_t}-\frac{1}{P_f} \quad \text{(eq. 2)}$$

For transmission electron microscopy, the same setup used for *in vitro* transcytosis experiment was performed. B16/F10 cells were cultured with each formulation of HAuNS (without radiolabeling) for 30 min at 37°C. The cell culture insert membrane with the cells was then washed and fixed with a cocktail containing 2% paraformaldehyde and 3% glutaraldehyde. The membrane with the cells was cut perpendicularly and prepared using standard procedures for biological samples.

2.6. MicroPET imaging and histology analysis

The animals used for the experiment were treated according to protocols evaluated and approved by the Institutional Animal Care and Use Committee of The University of Texas MD Anderson Cancer Center. Nude mice (female, 6–8 weeks) were inoculated subcutaneously with 5×10^5 B16/F10 melanoma cells 10 days before the experiment. Tumor-bearing mice were randomly allocated into 5 groups (n = 3) and injected intravenously with 7.5 mCi/kg ^{64}Cu-labeled HAuNS conjugates with or without the presence of 500 μg of Ant-PEG-SATA (blocking). The animals were anesthetized with 2% isofluorane (Baxter), and microPET images were acquired 1, 4, and 24 h after radiotracer injection using a Rodent R4 microPET scanner (Concorde Microsystems, Inc.). After the experiments, the mice were euthanized with CO_2. PET images were reconstructed using ASIPro VM 6.3.3.0 software (Concorde Microsystems, Inc). Counts per pixel per minute in the regions of interest were converted to microcuries using a calibration curve derived from scanning standard activity

phantoms in the microPET scanner. Uptake of ^{64}Cu-labeled HAuNS in each tumor was divided by the volume of the tumor to obtain percentage injected dose per cubic centimeter (%ID/cm^3).

In a separate experiment, tetramethylrhodamine-labeled HAuNS conjugates were injected intravenously into tumor-bearing mice, with or without the presence of 500 μg of pegylated Ant (Ant-PEG, blocking). The animals were euthanized 4 and 24 h after injection. Tumors were resected for frozen sectioning. The tumor tissue was stained with rat anti-mouse CD31 monoclonal antibody and rabbit anti-MC1R polyclonal antibody (Millipore) and then with IRDye680 goat anti-rat IgG (Li-Cor) and Alexa Fluor 488-conjugated goat anti-rabbit IgG (Invitrogen). Cell nuclei were counterstained with 4′,6-diamidino-2-phenylindole (DAPI). The slices were examined under a fluorescence microscope (Zeiss).

3. Results and Discussion

3.1. MC1R binding affinity of different HAuNS conjugates

We used HAuNS as a model nanoparticle-based delivery system. For the MC1R agonist targeting moiety, we chose melanocyte-stimulating hormone analog [Nle^4,D-Phe^7]-α-MSH (NDP-α-MSH, referred to as *Ago*). NDP-α-MSH is a 13-amino-acid peptide that had high binding affinity to MC1R (IC_{50}=2.09×10^{-10} M, Fig. 1B). For the MC1R antagonist targeting moiety, we chose human agouti-related protein 109–118 [hAGRP (109–118), referred to as *Ant*]. AGRPs antagonize G protein-coupled receptors (GPCRs) [20, 21]. Structure-function studies of hAGRP(109–118) decapeptide modified with lactam bridge resulted in the identification of this peptide as an MC1R antagonist [22, 23]. This peptide also had high binding affinity to MC1R (IC_{50}=2.31×10^{-8} M, Fig. 1B).

It was previously reported that ligand-conjugated nanoparticles provided for multivalent binding, leading to receptor affinities orders of magnitude higher than those with free ligand [24]. Our results showed that the binding affinity of Ago-PEG-HAuNS and Ant-PEG-HAuNS to MC1R could be tuned by adjusting the density of ligands on the nanoparticle surface (Fig. 1C). Although the MC1R binding affinity of free Ago was 2 orders of magnitude higher than that of free Ant, HAuNS with an average of 39 Ago attached per nanoparticle (Ago39-PEG-HAuNS) and HAuNS with an average of 367 Ant_9 attached per nanoparticle (Ant367-PEG-HAuNS) had similar binding affinity to MC1R (IC_{50}=2.31×10^9 particles/ml and IC_{50}=1.12×10^9 particles/ml, respectively). We thus used Ago39-PEG-HAuNS and Ant367-PEG-HAuNS in the subsequent comparative studies. The binding similarity was considered a prerequisite for thorough comparison of the 2 nanoparticle formulations in this study. We anticipated that MC1R agonist-conjugated HAuNS (Ago-PEG-HAuNS) would be internalized upon ligand-receptor binding and that MC1R antagonist-conjugated HAuNS (Ant-PEG-HAuNS) would remain attached on the cell surface.

3.2. Intracellular trafficking

To further study nanoparticle-receptor interaction and intracellular trafficking of targeted nanoparticles, we created HEK 293 cells expressing a chimeric protein comprised of MC1R and GFP, referred to as MC1R-GFP. HAuNS were labeled with tetramethylrhodamine fluorescent probe through a PEG linker. As observed on confocal microscopy, in HEK 293 cells transiently transfected with *MC1R-GFP*-encoding plasmid DNA, the green fluorescence of MC1R-GFP was distributed evenly along the cell membrane. Addition of fluorescence-labeled Ago39-PEG-HAuNS caused translocation of both receptor and nanoparticle into intracellular compartments, which was evidenced by the colocalization of fluorescence signals from MC1R-GFP and HAuNS (Fig. 2, arrows). Addition of an excessive amount of free Ant completely inhibited the nanoparticle-receptor interaction as

well as Ago39-PEG-HAuNS-mediated receptor internalization. In contrast, Ant367-PEG-HAuNS bound to and colocalized with MC1R-GFP on the cell surface but did not stimulate receptor internalization (Fig. 2, arrowheads). Like Ago39-PEG-HAuNS binding, Ant367-PEG-HAuNS's binding to MC1R-GFP was inhibited by an excessive amount of free Ant. The nontargeted PEG-HAuNS showed less membrane binding and cellular uptake than targeted HAuNS. There was no overlap in fluorescence signals between PEG-HAuNS and MC1R-GFP, suggesting that PEG-HAuNS were taken up by the cells via nonspecific process. These results indicated that MC1R mediated endocytosis of Ago39-PEG-HAuNS but not Ant367-PEG-HAuNS.

Since MC1R is a member of the GPCR superfamily and it is well known that β-arrestin serves as an adapter linking activated GPCRs to the downstream cellular trafficking machinery (clathrin, AP-2 complexes) [25, 26], we used immunohistochemical staining to track the cellular distribution of β-arrestin and clathrin in B16/F10 melanoma cells after binding by tetramethylrhodamine-labeled targeted HAuNS. We found that stimulation of MC1R by Ago39-PEG-HAuNS triggered rapid β-arrestin recruitment to the cell surface and colocalization with the nanoparticles. Further, the HAuNS and β-arrestin signals overlapped well with clathrin staining (Fig. S2, top row). In contrast, most Ant367-PEG- HAuNS did not trigger β-arrestin recruitment and remained on the cell membrane 30 min after treatment (Fig. S2, middle row). The nontargeted PEG-HAuNS showed less cellular binding and internalization, which was unrelated to either β-arrestin or clathrin (Fig. S2, bottom row). Previous studies using 2-photon fluorescence laser scanning microscopy showed that agonist-mediated internalization of all subtypes of melanocortin receptors is dependent on β-arrestin-mediated clathrin-coated pits [9, 10]. Our findings proved that upon agonist-receptor binding, β-arrestin recruitment was a key step of the GPCR-activated cell signaling pathway to trigger internalization of HAuNS through clathrin-coated pits.

We next examined downstream cAMP signaling upon nanoparticle-MC1R interaction. In agreement with previous reports that Ago peptide is a potent agonist of MC1R [27], adenylyl cyclase assay showed significant increase of intracellular cAMP accumulation when B16/F10 cells were incubated with Ago39-PEG-HAuNS (Fig. S3). The Ago39-PEG-HAuNS-induced cAMP increase was completely abolished by free Ant. In contrast, there was no effect of Ant367-PEG-HAuNS on cAMP signaling following cellular binding.

To further evaluate differential cellular responses upon nanoparticle binding to MC1R, we used high-resolution AFM to analyze topographic changes of the cellular membrane in B16/F10 cells before and after nanoparticles treatment. The control cells without any treatment spread on glass surface with height ranging from 4.1 to 5.7 μm, and contact area of 1493 to 4166 μm^2 (Fig. 3A). A deflection image (Fig. 3B) revealed that the cellular membrane was relatively rough, with clusters ranging from 0.3 to 2.5 μm in height and 1.7 to 13.0 μm laterally. The flat region surrounding the clusters had roughness of 38.7 nm (Fig. 3C, cursor profile 2). The cells treated with Ago39-PEG-HAuNS (Fig. 3D–F) exhibited a different morphology with a lower level of spreading, with height ranging from 4.5 to 7.7 μm, and contact area of 793 to 1452 μm^2. The cell membranes exhibited high density of craters; 33 craters were detected in a selected 30 μm × 30 μm area (Fig. 3F, arrows). The width of these craters ranged from 0.7 to 3.1 μm, and the depth ranged from 0.4 to 1.1 μm (cursor profiles 4 and 5). The presence of these craters on cell membrane suggested endocytosis of the nanoparticles by cells treated with Ago39-PEG-HAuNS. The cells treated with Ant367-PEG-HAuNS (Fig. 3G–I) exhibited a similar degree of spreading to that observed in the Ago39-PEG-HAuNS-treated cells. High resolution view is dominated by clusters ranging from 0.5 to 1.2 μm in height and 1.4 to 4.2 μm laterally (cursor profile 7). The image revealed detailed membrane structure differs from the Ago39-PEG-HAuNS treatments. Although craters were also observed (Fig. 3I), they were much smaller than the craters in the

cells treated with Ago39-PEG-HAuNS. The width of these craters ranged from 0.4 to 1.2 μm, the depth ranged from 0.1 to 0.2 μm (cursor profile 8), and only 8 craters were detected in a selected 30 μm × 30 μm area. These results indicated that most Ant367-PEG-HAuNS remained bound to the cellular surface.

3.3 MC1R-mediated transcytosis of HAuNS in tumor cells

To understand the effect of the MC1R-targeting ligands on transport of HAuNS through tumor cells, we established an *in vitro* tumor cell permeation model (Fig. 4A). The calculation of permeability (*P*), standing for the rate of nanoparticle transport from the apical (donor) compartment to the basolateral (receiver) compartment, has previously been used to evaluate the trans-endothelial transport of nanoparticles [16, 28]. Unlike the endothelial cells forming monolayer with intercellular tight junction [16, 28], the B16/F10 tumor cells formed multi-cell layers on the membrane of the insert without intercellular tight junction. Quantitative analysis of movement of ^{64}Cu-labeled HAuNS across the B16/F10 multilayer (P_c) showed that Ago39-PEG-HAuNS had a rate of cell penetration 3.27 times that of PEG-HAuNS (Fig. 4B). The P_c of nontargeted PEG-HAuNS represents paracellular transport and nonspecific intracellular transport of the nontargeted HAuNS (e.g., pinocytosis). The increased P_c of Ago39-PEG-HAuNS could be attributed to MC1R-mediated transcytosis induced by Ago. The increase of Ago-triggered transcytosis was almost completely blocked by free Ant. Ant367-PEG-HAuNS did not display an increased rate of cell penetration compared with nontargeted PEG-HAuNS (Fig. 4B), suggesting that the interaction between MC1R and Ant cannot induce receptor-mediated transcytosis. This was confirmed by transmission electron microscopy findings, shown in Fig. 4C. PEG-HAuNS without MC1R targeting ligand bound to the cellular surface, and only a few nanoparticles were internalized. Ant367-PEG-HAuNS similarly bound to the cellular surface with only a few nanoparticles internalized. However, Ago39-PEG-HAuNS exhibited significant endocytosis (Fig. 4C, bottom row). Uptake of Ago39-PEG-HAuNS occurred at the luminal (apical) cytoplasmic membrane via receptor-mediated endocytosis (Fig. 4C, asterisks). Endocytic vesicles were transported toward the basolateral cytoplasmic membrane (Fig. 4C, arrows). Evidence also showed exocytosis of Ago39-PEG-HAuNS through the membrane pores of the cell culture insert to the receiver compartment (Fig. 4C, arrowheads). Taken together, these findings indicated that the 2 different types of nanoparticles mediated different cellular processes with respect to cellular internalization, recruitment of adapter protein, and activation of cAMP signaling. The strong *in vitro* evidence of transcytosis triggered by Ago39-PEG-HAuNS suggested that Ago39-PEG-HAuNS may display an *in vivo* transport pattern different from that of Ant367-PEG-HAuNS after their extravasation from the tumor blood vessels.

To test this concept, we investigated the tumor biodistribution of ^{64}Cu-labeled HAuNS in nude mice bearing B16/F10 melanoma by microPET. At 1 h following systemic administration, tumor accumulation of Ago39-PEG-HAuNS was significantly higher than tumor accumulation of Ant367-PEG-HAuNS and PEG-HAuNS ($P<0.05$) (Fig. 5A and 5B). Tumor localization of Ago39-PEG-HAuNS at 4 h and 24 h after injection was about twice that of PEG-HAuNS. Co-injection of pegylated Ant inhibited this increased tumor uptake. In contrast, tumor accumulation of Ant367-PEG-HAuNS at 1, 4, and 24 h after injection was not significantly different from that of PEG-HAuNS.

Immunofluorescence tracking further confirmed the significantly enhanced tumor distribution of Ago39-PEG-HAuNS compared to the other two HAuNS formulations at 4 and 24 h after injection (Figure 5c, top and middle rows). Pegylated Ant inhibited this localization, indicating active targeting of Ago39-PEG-HAuNS. To our delight, Ago39-PEG-HAuNS were transported far beyond the microvessels at both 4 h and 24 h, while Ant367-PEG-HAuNS and PEG-HAuNS remained mostly located in the perivascular region

at 4 h and 24 h (Fig. 5C, top row). At higher magnification (Fig. 5C, bottom row), micrographs revealed that most nontargeted PEG-HAuNS were distributed in the extracellular space. Ant367-PEG-HAuNS were bound to MC1R on the tumor cell membrane. In both cases, MC1R was evenly distributed throughout the tumor volume. In contrast, Ago39-PEG-HAuNS were internalized together with MC1R in tumor cells, suggesting receptor-mediated endocytosis (Fig. 5C, arrows).

The different distribution patterns of Ago39-PEG-HAuNS and Ant367-PEG-HAuNS in the tumor interstitium support a mechanism of enhanced intratumoral transport of nanoparticles through receptor-mediated transcytosis (Fig. 6). As exemplified in the MC1R system, when agonist-conjugated HAuNS bind to MC1R, the receptors are phosphorylated and activated, which leads to β-arrestin recruitment. The receptor-bound β-arrestin acts as an endocytic adapter, which in turn binds to components of the clathrin endocytic machinery. This leads to the formation of clathrin-coated pits to engulf the receptor-nanoparticle complex. Upon internalization, β-arrestin rapidly dissociates from MC1R, and the receptor-nanoparticle complex is trafficked to an endosomal compartment, wherein the ligand is dissociated and the receptor dephosphorylated [29]. The endocytic vesicles containing both receptors and nanoparticles are subsequently transported either to the luminal plasma membrane, where the receptors are recycled, or to the abluminal (basolateral) cytoplasmic membrane, where the nanoparticles are transcytosized (Fig. 6A). The interaction between MC1R and antagonist-conjugated HAuNS, on the other hand, cannot mediate endocytosis, and the targeted nanoparticle remains attached on the cell surface.

The proposed transcytosis trafficking mechanism helps us explain improved extravascular transport and enhanced tumor uptake of agonist-conjugated HAuNS (Fig. 6B). Following extravasation from the tumor vasculature, nontargeted PEG-HAuNS accumulate in the perivascular region owing to the EPR effect. Our fluorescent micrographs have shown that PEG-HAuNS penetrate only a few cell diameters into the extravascular tumor tissue (Fig. 5C), which is in line with previous reports in the literature [30, 31]. Similarly, antagonist-conjugated HAuNS mostly accumulate in the perivascular region, although some Ant-PEG-HAuNS do bind to the tumor cells, whereas PEG-HAuNS localize in the extracellular matrix. In contrast, agonist-conjugated HAuNS are transported via receptor-mediated transcytosis, an active transport process that promotes dispersion of nanoparticles far from the tumor vessels (Fig. 6).

Significant effort has been spent in the past decades on developing a targeted, long-circulating nanoparticle formulation. However, active targeting of nanoparticles to the tumor interstitium is a complicated, multifactorial issue. Comprehensive studies that carefully dissect various processes involved in delivery of systemically administered nanoparticles to cells in solid tumors, including distribution through the vascular compartment, transport across the microvascular wall, and dispersion within tumors, are needed to address some of the conflicting data in the literature. It is expected that the emergence of new nanotechnologies will facilitate the development of delivery systems that can efficiently deliver nanoparticles to tumors.

5. Conclusion

The nature of targeting ligands, i.e., whether they are agonists or antagonists, directs tumor uptake and intratumoral distribution after extravasation of nanoparticles from tumor vessels into the extravascular fluid space. We used MC1R as a model tumor marker to elucidate receptor-mediated transcytosis of nanoparticles in solid tumors. Active extravascular transport of nanoparticles was initiated by internalization upon agonist-receptor, but not antagonist-receptor, binding followed by transcellular transport by tumor cells.

Supplementary Material

Refer to Web version on PubMed Central for supplementary material.

Acknowledgments

We thank Stephanie Deming for editing the manuscript. This work was supported in part by grants from the National Institutes of Health (grant R01 CA119387–05S1 and RC2 GM092599), by the John S. Dunn Foundation, and W. M. Keck Foundation. The Transmission Electron Microscopy facility is supported by the National Institutes of Health through MD Anderson's Cancer Center Support Grant, CA016672. The ^{64}Cu was provided by Washington University Medical School, which is partially funded through National Cancer Institute grant R24 CA86307.

References

1. Sanhai WR, Sakamoto JH, Canady R, Ferrari M. Seven challenges for nanomedicine. Nat Nanotechnol. 2008; 3:242–244. [PubMed: 18654511]
2. Pirollo KF, Chang EH. Does a targeting ligand influence nanoparticle tumor localization or uptake? Trends Biotechnol. 2008; 26:552–558. [PubMed: 18722682]
3. Huang X, Peng X, Wang Y, Shin DM, El-Sayed MA, Nie S. A reexamination of active and passive tumor targeting by using rod-shaped gold nanocrystals and covalently conjugated peptide ligands. ACS Nano. 2010; 4:58875896.
4. Bartlett DW, Su H, Hildebrandt IJ, Weber WA, Davis ME. Impact of tumor-specific targeting on the biodistribution and efficacy of siRNA nanoparticles measured by multimodality in vivo imaging. Proc Natl Acad Sci U S A. 2007; 104:15549–15554. [PubMed: 17875985]
5. Kirpotin DB, Drummond DC, Shao Y, Shalaby MR, Hong K, Nielsen UB, Marks JD, Benz CC, Park JW. Antibody targeting of long-circulating lipidic nanoparticles does not increase tumor localization but does increase internalization in animal models. Cancer Res. 2006; 66:6732–6740. [PubMed: 16818648]
6. Melancon MP, Lu W, Yang Z, Zhang R, Cheng Z, Elliot AM, Stafford J, Olson T, Zhang JZ, Li C. In vitro and in vivo targeting of hollow gold nanoshells directed at epidermal growth factor receptor for photothermal ablation therapy. Mol Cancer Ther. 2008; 7:1730–1739. [PubMed: 18566244]
7. Siegrist W, Solca F, Stutz S, Giuffre L, Carrel S, Girard J, Eberle AN. Characterization of receptors for alpha-melanocyte-stimulating hormone on human melanoma cells. Cancer Res. 1989; 49:6352–6358. [PubMed: 2804981]
8. Miao Y, Benwell K, Quinn TP. 99mTc- and 111In-labeled alpha-melanocyte-stimulating hormone peptides as imaging probes for primary and pulmonary metastatic melanoma detection. J Nucl Med. 2007; 48:73–80. [PubMed: 17204701]
9. Cai M, Varga EV, Stankova M, Mayorov A, Perry JW, Yamamura HI, Trivedi D, Hruby VJ. Cell signaling and trafficking of human melanocortin receptors in real time using two-photon fluorescence and confocal laser microscopy: differentiation of agonists and antagonists. Chem Biol Drug Des. 2006; 68:183–193. [PubMed: 17105482]
10. Cai M, Stankova M, Pond SJ, Mayorov AV, Perry JW, Yamamura HI, Trivedi D, Hruby VJ. Real time differentiation of G-protein coupled receptor (GPCR) agonist and antagonist by two photon fluorescence laser microscopy. J Am Chem Soc. 2004; 126:7160–7161. [PubMed: 15186137]
11. Lu W, Xiong C, Zhang G, Huang Q, Zhang R, Zhang JZ, Li C. Targeted photothermal ablation of murine melanomas with melanocyte-stimulating hormone analog-conjugated hollow gold nanospheres. Clin Cancer Res. 2009; 15:876–886. [PubMed: 19188158]
12. Lu W, Zhang G, Zhang R, Flores LG 2nd, Huang Q, Gelovani JG, Li C. Tumor site-specific silencing of NF-kappaB p65 by targeted hollow gold nanosphere-mediated photothermal transfection. Cancer Res. 2010; 70:3177–3188. [PubMed: 20388791]
13. Grieco P, Cai M, Han G, Trivedi D, Campiglia P, Novellino E, Hruby VJ. Further structure-activity studies of lactam derivatives of MT-II and SHU-9119: their activity and selectivity at human melanocortin receptors 3, 4, and 5. Peptides. 2007; 28:1191–1196. [PubMed: 17482720]

14. Zink T, Deng Z, Chen H, Yu L, Liu FT, Liu GY. High-resolution three-dimensional imaging of the rich membrane structures of bone marrow-derived mast cells. Ultramicroscopy. 2008; 109:22–31. [PubMed: 18790570]
15. Deng Z, Zink T, Chen HY, Walters D, Liu FT, Liu GY. Impact of actin rearrangement and degranulation on the membrane structure of primary mast cells: a combined atomic force and laser scanning confocal microscopy investigation. Biophys J. 2009; 96:1629–1639. [PubMed: 19217878]
16. Roger E, Lagarce F, Garcion E, Benoit JP. Lipid nanocarriers improve paclitaxel transport throughout human intestinal epithelial cells by using vesicle-mediated transcytosis. J Control Release. 2009; 140:174–181. [PubMed: 19699246]
17. D'Souza VM, Shertzer HG, Menon AG, Pauletti GM. High glucose concentration in isotonic media alters caco-2 cell permeability. AAPS PharmSci. 2003; 5:E24. [PubMed: 14621959]
18. Lundquist S, Renftel M, Brillault J, Fenart L, Cecchelli R, Dehouck MP. Prediction of drug transport through the blood-brain barrier in vivo: a comparison between two in vitro cell models. Pharm Res. 2002; 19:976–981. [PubMed: 12180550]
19. Cecchelli R, Dehouck B, Descamps L, Fenart L, Buee-Scherrer VV, Duhem C, Lundquist S, Rentfel M, Torpier G, Dehouck MP. In vitro model for evaluating drug transport across the blood-brain barrier. Adv Drug Deliv Rev. 1999; 36:165–178. [PubMed: 10837714]
20. Shutter JR, Graham M, Kinsey AC, Scully S, Luthy R, Stark KL. Hypothalamic expression of ART, a novel gene related to agouti, is up-regulated in obese and diabetic mutant mice. Genes Dev. 1997; 11:593–602. [PubMed: 9119224]
21. Ollmann MM, Wilson BD, Yang YK, Kerns JA, Chen Y, Gantz I, Barsh GS. Antagonism of central melanocortin receptors in vitro and in vivo by agouti-related protein. Science. 1997; 278:135–138. [PubMed: 9311920]
22. Thirumoorthy R, Holder JR, Bauzo RM, Richards NG, Edison AS, Haskell-Luevano C. Novel agouti-related-protein-based melanocortin-1 receptor antagonist. J Med Chem. 2001; 44:4114–4124. [PubMed: 11708914]
23. Sharov AA, Fessing M, Atoyan R, Sharova TY, Haskell-Luevano C, Weiner L, Funa K, Brissette JL, Gilchrest BA, Botchkarev VA. Bone morphogenetic protein (BMP) signaling controls hair pigmentation by means of cross-talk with the melanocortin receptor-1 pathway. Proc Natl Acad Sci U S A. 2005; 102:93–98. [PubMed: 15618398]
24. Hild W, Pollinger K, Caporale A, Cabrele C, Keller M, Pluym N, Buschauer A, Rachel R, Tessmar J, Breunig M, Goepferich A. G protein-coupled receptors function as logic gates for nanoparticle binding and cell uptake. Proc Natl Acad Sci U S A. 2010; 107:10667–10672. [PubMed: 20498042]
25. Shenoy SK, Lefkowitz RJ. Multifaceted roles of beta-arrestins in the regulation of seven-membrane-spanning receptor trafficking and signalling. Biochem J. 2003; 375:503–515. [PubMed: 12959637]
26. Lefkowitz RJ, Shenoy SK. Transduction of receptor signals by beta-arrestins. Science. 2005; 308:512–517. [PubMed: 15845844]
27. Sawyer TK, Sanfilippo PJ, Hruby VJ, Engel MH, Heward CB, Burnett JB, Hadley ME. 4-Norleucine, 7-D-phenylalanine-alpha-melanocyte-stimulating hormone: a highly potent alpha-melanotropin with ultralong biological activity. Proc Natl Acad Sci U S A. 1980; 77:5754–5758. [PubMed: 6777774]
28. Lu W, Tan YZ, Hu KL, Jiang XG. Cationic albumin conjugated pegylated nanoparticle with its transcytosis ability and little toxicity against blood-brain barrier. Int J Pharm. 2005; 295:247–260. [PubMed: 15848009]
29. Luttrell LM, Lefkowitz RJ. The role of beta-arrestins in the termination and transduction of G-protein-coupled receptor signals. J Cell Sci. 2002; 115:455–465. [PubMed: 11861753]
30. Hambley TW, Hait WN. Is anticancer drug development heading in the right direction? Cancer Res. 2009; 69:1259–1262. [PubMed: 19208831]
31. Ruoslahti E, Bhatia SN, Sailor MJ. Targeting of drugs and nanoparticles to tumors. J Cell Biol. 2010; 188:759–768. [PubMed: 20231381]

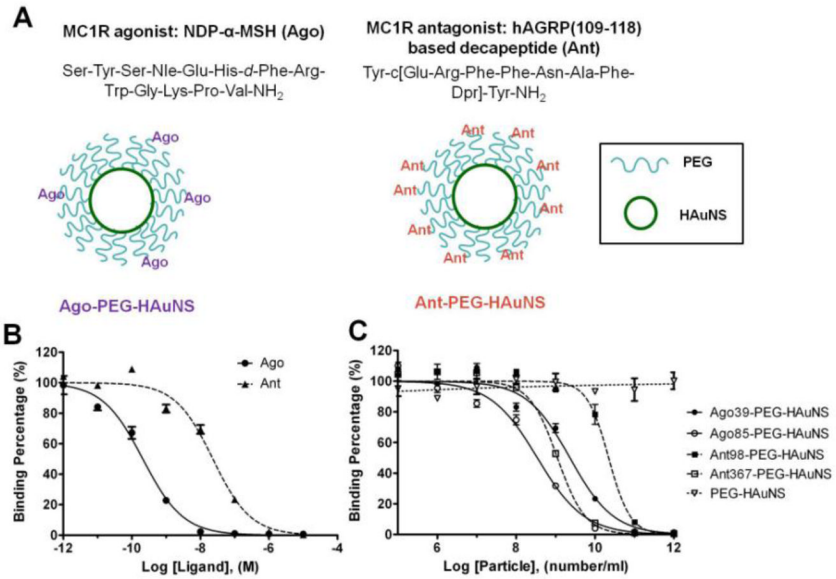

Fig. 1.

(A) Chemical structure of MC1R agonist (Ago) and antagonist (Ant) and schemes of bioconjugation. (B) Competitive binding assay comparing ^{125}I-NDP-α-MSH with unlabeled Ago or Ant. (C) Competitive binding assay comparing ^{125}I-NDP-α-MSH with unlabeled Ago- or Ant-conjugated pegylated HAuNS. Ago39 and Ago85 had an average of 39 and 85 agonists, respectively, conjugated per nanoparticle. Ant98 and Ant367 had an average of 98 and 367 antagonists, respectively, conjugated per nanoparticle.

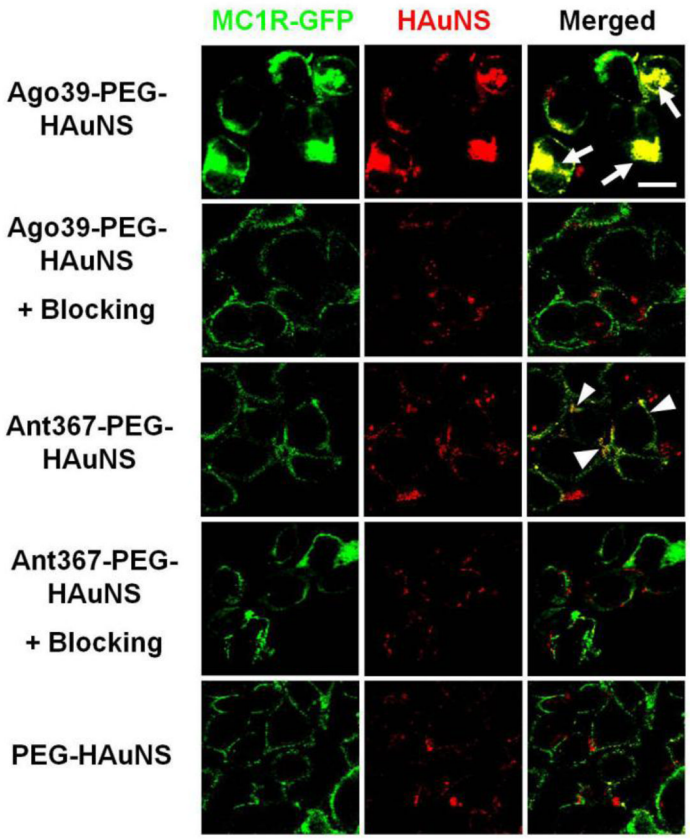

Fig. 2.

Intracellular localization of tetramethylrhodamine-labeled PEG-HAuNS, Ago39-PEG-HAuNS, or Ant367-PEG-HAuNS (red) in HEK 293 cells transfected with *MC1R-GFP* coexpression plasmid (green) after 20 min incubation at 37°C, with or without the presence of 200 μg/ml free Ant (blocking). Arrows, overlap of green and red fluorescence in cytoplasm; Arrowheads, overlap of green and red fluorescence on cell membrane. Bar, 20 μm.

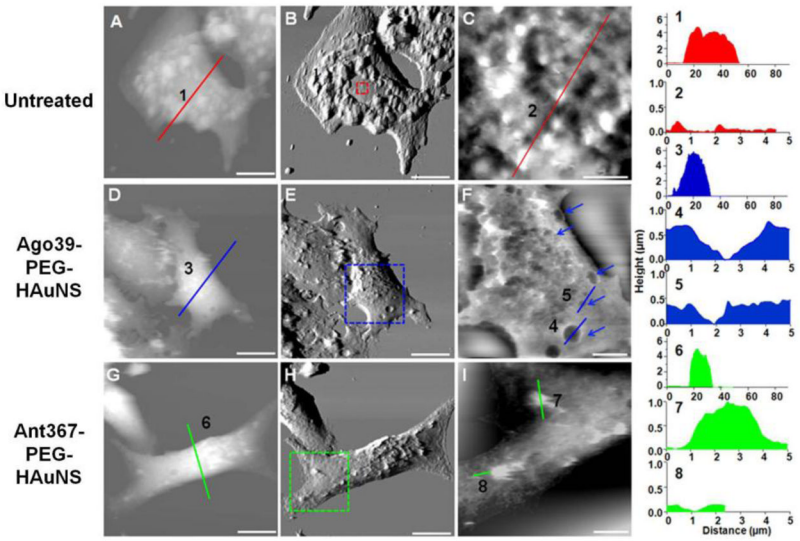

Fig. 3.

AFM images reveal 3-dimensional membrane structural features of B16/F10 melanoma cells after different treatments. (A) A 90 μm × 90 μm atomic force microscopy topograph of a typical B16/F10 melanoma cell. (B) Deflection image corresponding to the image in (A). (C) Zoom-in view of the framed region in (B). Cursor profiles 1 and 2 at the right correspond to cursors 1 and 2 in (A) and (C), respectively. The displays in the middle and bottom rows follow the same organization as used in the top row, for Ago39-PEG-HAuNS-treated and Ant367-PEG-HAuNS-treated B16/F10 cells, respectively. Bars: (A), (B), (D), (E), (G), and (H), 20 μm; (C), 1 μm; (F) and (I), 5 μm. Arrows indicate craters.

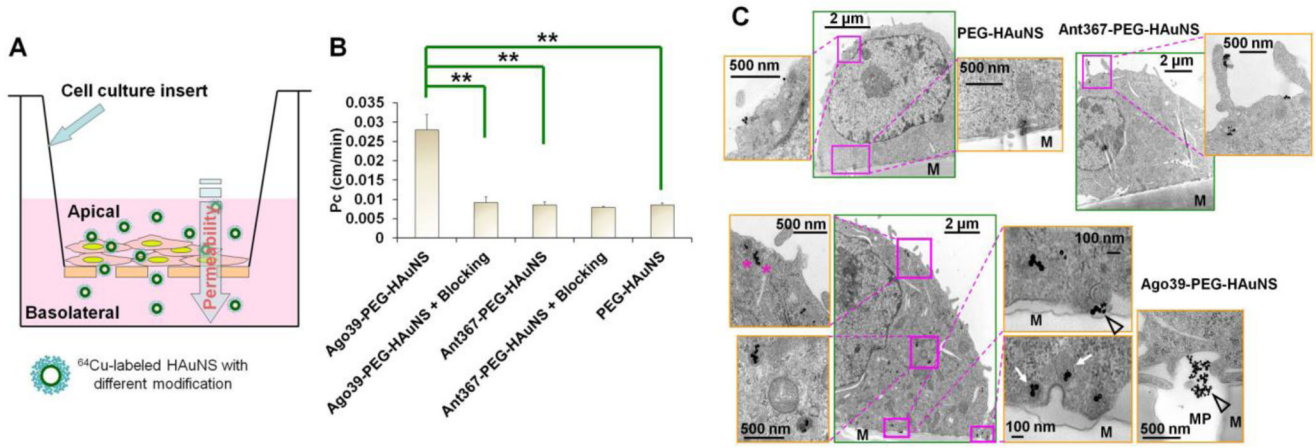

Fig. 4.

(A) Schematic drawing of *in vitro* B16/F10 melanoma cell multilayer for evaluation of HAuNS transcytosis. (B) Permeability of ^{64}Cu-labeled PEG-HAuNS, Ago39-PEG-HAuNS, or Ant367-PEG-HAuNS across the B16/F10 multilayer (P_c) with or without the presence of 200 μg/ml of free Ant (blocking), n=3. (C) Transmission electron micrographs of intracellular distribution of nontargeted PEG-HAuNS and PEG-HAuNS with different MC1R targeting moieties. M represents cell culture membrane. MP represents membrane pore. Asterisks represent endocytosis of nanoparticles at luminal cytoplasmic membrane. Arrows represent transcytosis of nanoparticle-incorporated vesicles toward basolateral cytoplasmic membrane. Arrowheads represent exocytosis of nanoparticles.

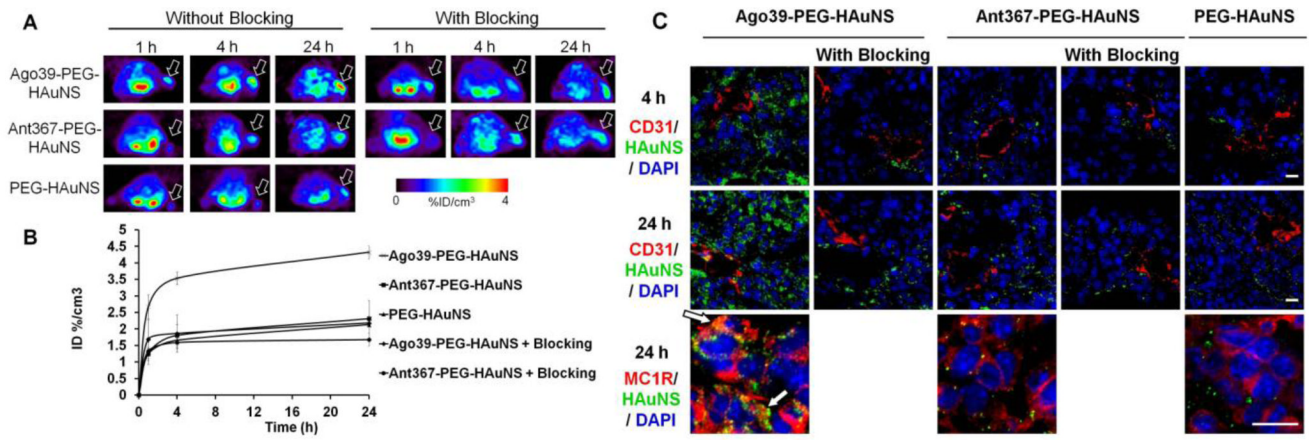

Fig. 5.

Targeting B16/F10 melanoma in a mouse model. (A) Representative microPET images at 1, 4, and 24 h after intravenous injection of ^{64}Cu-labeled PEG-HAuNS, Ago39-PEG-HAuNS, or Ant367-PEG-HAuNS with or without the presence of 500 μg of pegylated Ant (blocking), n=3. Arrows, tumor. (B) Quantitative analysis of tumor uptake of ^{64}Cu-labeled HAuNS, n=3. (C) Immunofluorescence micrographs of tumor tissue following nanoparticle injection. Bars, 20 μm. Arrows, colocalization of Ago39-PEG-HAuNS with internalized MC1R.

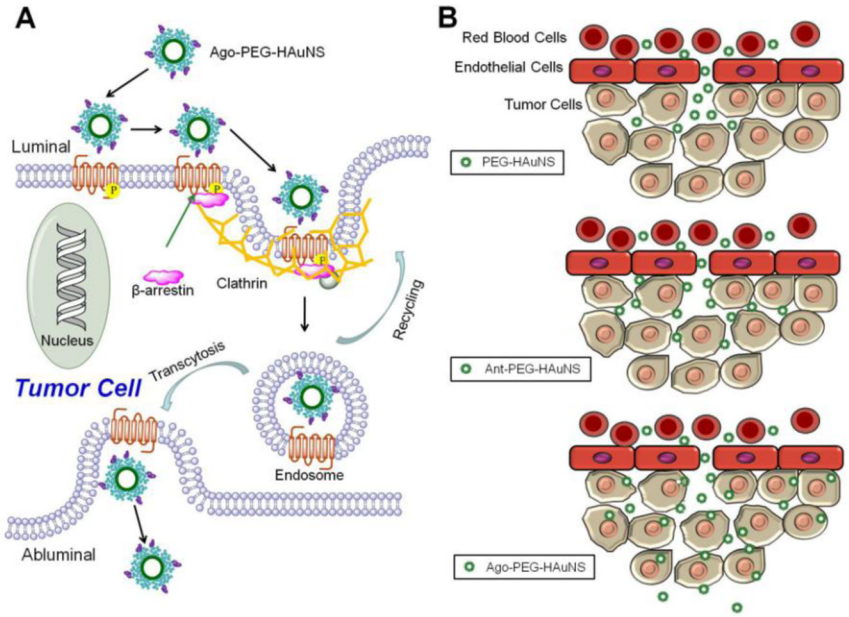

Fig. 6.

(A) Scheme for transcytosis of MC1R agonist-conjugated HAuNS. (B) Schematic illustration showing the mechanism of tumor targeting through delivery of nanoparticles with different homing ligands on surface.